PHD Thesis

Something something

something

SABRE

Philipp Rovedo

Examiner: Prof. Dr. Jürgen Hennig
Adviser: Prof Dr. Jan Hövener

Albert-Ludwigs-University Freiburg
Faculty of Physics
Department of Radiology
Chair for Medical Physics

October 05th, 2017

Writing period

05. 07. 2017 – 05. 10. 2017

Examiner

Prof. Dr. Jürgen Hennig

Advisers

PD Dr. Jan Hövener

Declaration

I hereby declare, that I am the sole author and composer of my thesis and that no other sources or learning aids, other than those listed, have been used. Furthermore, I declare that I have acknowledged the work of others by providing detailed references of said work.
I hereby also declare, that my Thesis has not been prepared for another examination or assignment, either wholly or excerpts thereof.

_____   _____
Place, Date   Signature

Abstract

foo bar

Contents

List of Figures

List of Tables

List of Algorithms

398.33864pt

1 Introdduction

1.1 setup.tex

Edit setup.tex according to your needs. The file contains two sections, one for package includes, and one for defining commands. At the end of the includes and commands there is a section that can safely be removed if you don't need algorithms or tikz. Also don't forget to adapt the pdf hypersetup!!
setup.tex defines:

- some new commands for remembering to do stuff:
  - \todo{Do this!}: **(TODO: Do this!)**
  - \extend{Write more when new results are out!}:
    (EXTEND: Write more when new results are out!)
  - \draft{Hacky text!}: **(DRAFT: Hacky text!)** [1]

- some commands for referencing, 'in \chapref{chap:introduction}' produces 'in Chapter 1'
  - \chapref{}
  - \secref{sec:XY}
  - \eqref{}
  - \figref{}
  - \tabref{}

- the colors of the Uni's corporate design, accessible with {\color{UniX} Colored Text}
  - UniBlue
  - UniRed
  - UniGrey

- a command for naming matrices `\mat{G}`, $\mathbf{G}$, and naming vectors `\vec{a}`, $\mathbf{a}$. This overwrites the default behavior of having an arrow over vectors, sticking to the naming conventions normal font for scalars, bold-lowercase for vectors, and bold-uppercase for matrices.

- named equations:

```
\begin{align}
d(a,b) &= d(b,a)\\ \eqname{symmetry}
\end{align}
```

$$d(a, b) = d(b, a) \tag{1}$$

symmetry

2 Theory

2.1 NMR

Nuclear Magnetic Resonance (NMR) is a technique that emerged in 1946 with the discovery of the absortion properties of nuclei irradiated with electromagnetic waves resonant to their larmor frequencies.[2] The subsequent observation of signal from those previously excited nuclei, known as free induction decay (FID) paved the road to the now well established method which in the beginning was primarily used in chemistry for structural analysis of Molecules and chemical kinetics.

2.1.1 Larmor frequency

Inside an external magnetic field B_0, a magnetic dipole μ will precess with a frequency proportional to $B_0 \cdot \mu$. This also applies to charged particles with a spin $S \neq 0$ and thus a magnetic moment $\mu \neq 0$. The precession is a result of the torque $\mu \times \mathbf{B}$ excerted on the magnetic dipole moment.

2.1.2 Chemical shift

The larmor frequency of nuclei in NMR is largely governed by B_0 and μ, but other factors do influence it on a more subtle scale. The most prominent effect is the chemical shift which originates in the shielding of B_0 by the electrons' magnetic dilpoles surrounding the nucleus or molecule. The shielding thus generally leads to a decrease of precession frequency, the chemical shift though is calculated as the relative frequency quota towards another known sample's reference frequency:

$$\delta = \frac{\nu_{sample} - \nu_{reference}}{\nu_{reference}} \qquad (2)$$

2.1.3 J-coupling

In addition to the change in field by the electrons dipoles, the nucleis' magnetic dipoles inside one molecule will also interact. The interaction can be conveyed either directly or via the electrons' spins. The direct interaction is neglectable in liquids due to fastly rotating spins that average to zero. The indirect interaction via the electrons can also lead to a frequency shift resulting in multiplets usually on scales smaller than the chemical shifts, i.e. in the Hz range.

2.1.4 Flip angle

An external, on-resonant magnetic field will cause the magnetization of an ensemble of spins to flip by an angle α known as the flip angle (FA). An FA of $\mathrm{n} \cdot 180 \deg +90 \deg$ will rotate the magnetization to the transverse plane perpendicular to the magnetic field resulting in an FID. Pulses of $\mathrm{n} \cdot 180 \deg$ will keep the magnetization aligned with the magnetic field or invert it, therefore not resulting in a FID. All other FAs will produce a linear combination of the two cases.

2.1.5 A simple NMR experiment

The most basic experiment in NMR is the exposure of a spin ensemble to a $90°$ RF pulse and subsequent readout. This will flip the magnetization by $90°$ which will subsequently precess around the z axisi with its Larmor frequency. Using a coil**??** mounted around the sample, the alternating field caused by the rotating magnetization will induce a current driving the resonant circuit. That signal - or free induction decay - can be recorded as the voltage over the resonant circuit.

2.1.6 Relaxation

After being deflected from its thermal equilibrium, the magnetization tends to return to that equilibrium state. That process is called T_1 relaxation or spin-lattice relaxation and is an exponential decay. In addition, the transverse magnetization decays with a time constant called T_2 that is usually much smaller than T_1. T_2 relaxation is because of different magnetic fields experienced by the individual spins leading to a dephasing of the signal.

h **(TODO: T1/T2 figure)**

6

2.1.7 Field Gradients

For different purposes it is beneficial to not only have the homogeneous B_0 field, but also field gradients. Generally, these are additional z-fields that change linearly with one of the spatial dimentions. Generation of these fields is usually achieved by thermal conductors of specifically tailored geometries.

2.1.8 2D-NMR

2.2 Nuclei and Spins

The postulation of an electron spin in 1926 **??** and later in 1928 of a proton spin **??** opened up new areas of research.**(TODO: more history)** Individual spins can be described by their angular momentum operators $\hat{I}$, $\hat{I}_y$ and $\hat{I}_z$ that return the eigenvalue of the state in its respective direction.

$$\hat{I}_z \left| I, S \right\rangle = S \left| I, S \right\rangle \tag{3}$$

Considering a spin-1/2 particle in a magnetic field along the z-axis (e.g. the proton as a prominent particle in NMR), these eigenstates are

$$\left| \alpha \right\rangle = \begin{pmatrix} 1 \\ 0 \end{pmatrix} \qquad \left| \beta \right\rangle = \begin{pmatrix} 0 \\ 1 \end{pmatrix} \tag{4}$$

with the eigenvalues of $\pm 1/2$. Generally, every spin-1/2 particle can be in any superposition of those two eigenstates:

$$\left| \psi \right\rangle = c_\alpha \left| \alpha \right\rangle + c_\beta \left| \beta \right\rangle = \begin{pmatrix} c_\alpha \\ c_\beta \end{pmatrix} \tag{5}$$

Th;lkjsdfljk: thtlth:wqa :ese superposition states evolve under external conditions until a eigenstate of the particle is reached. Generally, a sample does not consist of one, but of many nuclei and thus many spins need to be described to describe the system. To do so, usually the density matrix formalism is introduced. It onsiders an ensembe of spins that do not interact with each other. In this case, the expectation value of an operator for a single spin $\langle \hat{Q} \rangle$ is given by

$$\left\langle \psi \right| \hat{Q} \left| \psi \right\rangle = \begin{pmatrix} c_\alpha^*, c_\beta^* \end{pmatrix} \begin{pmatrix} Q_{\alpha\alpha} Q_{\alpha\beta} \\ Q_{\beta\alpha} Q_{\beta\beta} \end{pmatrix} \begin{pmatrix} c_\alpha \\ c_\beta \end{pmatrix} \tag{6}$$

It can be shown that this is equal to the trace of the density operator $|\psi\rangle\langle\psi|$ multiplied with said operator

$$\langle\hat{Q}\rangle = \mathrm{Tr}\left\{|\psi\rangle\langle\psi|\hat{Q}\right\} \tag{7}$$

For multiple spins, it follows that the observable becomes the sum of their individual observables:

$$\langle\hat{Q}_{all}\rangle = \langle\psi_1|\hat{Q}|\psi_1\rangle + \langle\psi_2|\hat{Q}|\psi_2\rangle + \ldots = \mathrm{Tr}\left\{(|\psi_1\rangle\langle\psi_1| + \langle\psi_2||\psi_2\rangle + \ldots)\hat{Q}\right\} \tag{8}$$

This means that the system of spins can be described by the sum of the density operators called the density matrix

$$\hat{\rho} = \overline{|\psi\rangle\langle\psi|}. \tag{9}$$

For a spin-1/2 ensemble, the density matrix in thermal equilibrium is

$$\hat{\rho} = \begin{pmatrix} \frac{1}{2} + \frac{1}{4}\mathbb{B} & 0 \\ 0 & \frac{1}{2} - \frac{1}{4}\mathbb{B} \end{pmatrix} = \frac{1}{2}\hat{1} + \frac{1}{2}\mathbb{B}\hat{I}_z \tag{10}$$

with $\mathbb{B} = \frac{\hbar\gamma B_0}{k_b T}$. That means that in thermal equilibrium, the non-diagonal elements are zero, i.e. the socalled coherences (off-diagonal elements) are all equally populated while there is a slight overpopulation of one of the two states. Through deflection from that equilibrium, coherences are populated as described in the following section.

2.2.1 Radiofrequency pulses

Using the density matrix formalism, radiofrequency pulses described by rotational operators can be applied to the whole ensemble. A pulse $\hat{R}_\phi(\beta)$ of phase ϕ (corresponding to the axis around which magnetization is rotated) and angle β where $\beta = \omega_{nut} \cdot \tau_p$ exerting on a state $|\psi\rangle$ is described by

$$|\psi_\tau\rangle = \hat{R}_\phi(\beta)|\psi\rangle \tag{11}$$

Calculating the density matrix now leads to

$$\hat{\rho}_\tau = \overline{|\psi_\tau\rangle\langle\psi_\tau|} = \overline{\hat{R}_\phi(\beta)|\psi\rangle\langle\psi|\hat{R}_\phi(-\beta)} \tag{12}$$

8

where the overbar describes the averaging over all spins in the ensemble. Finally, as we are considering the same flip angle for every single spin in the ensemble, the formula can be reduced to

$$\hat{\rho}_\tau = \hat{R}_\phi(\beta)\hat{\rho}\hat{R}_\phi(-\beta) \tag{13}$$

meaning a rotation of the magnetization corresponds to a rotation of the desity matrix. If we consider a $90°$ pulse around the x axis on the previously described equilibrium for a spin-1/2 ensemble it follows:

$$\hat{\rho}_\tau = \hat{R}_x(\pi/2)\hat{\rho}\hat{R}_x(-\pi/2) = \frac{1}{2}\hat{1} + \frac{1}{2}\mathbb{B}\hat{R}_x(\pi/2)\hat{I}_z\hat{R}_x(-\pi/2)$$
$$= \begin{pmatrix} \frac{1}{2} & -\frac{1}{4i}\mathbb{B} \\ \frac{1}{4i}\mathbb{B} & \frac{1}{2} \end{pmatrix} \tag{14}$$

It can be equally shown that a $180°$ pulse inverts the populations of the diagonal elements while the coherences are untouched. If the system is not in thermal equilibrium, the states will evolve and generally relax back into the original equilibrium state. If one neglects said relaxation at first, the evolution can be described by **(TODO: ref formula rotationg frame)**

$$|\psi\rangle_\upsilon = \hat{R}_z(\Omega^0\upsilon)|\psi\rangle_\tau \text{ and}$$
$$\hat{\rho}_\upsilon = \hat{R}_z(\Omega^0\upsilon)\hat{\rho}_\tau\hat{R}_z(-\Omega^0\upsilon) \tag{15}$$

which shows that only a time dependent phase $\exp i\Omega^0\upsilon$ is added to the coherences and the populations stay constant. This confirms the macroscopic observation that the ensemble of spins behaves like a rotating vector of magnetization in the x-y-plane (w\o relaxation). If relaxation is added to the scheme, we can differentiate between relaxation of the coherences (T_2 relaxation) and that of the states (T_1 relaxation). The former affects the non diagonal elements only which will deacy to zero while the latter brings the populations of the states back to thermal equilibrium. That can be expressed by

$$\rho_{ij,\upsilon} = \rho_{ij,\tau}\exp\left(\pm i\Omega^0 - \lambda\right)\upsilon,\ \mathrm{i,j}\ =\ 1,2(+) \text{ or } 2,1(-) \tag{16}$$

for the non diagonal elements and

$$\rho_{ii,\upsilon} = (\rho_{ii,\tau} - \rho_{ii}^{eq})\exp(-\tau/T_1) + \rho_{ii}^{eq} \tag{17}$$

2.3 MRI

A huge addition to the world of NMR was the invention of spatially resolved sample maps, i.e. imaging. It was made possible through the clever use of gradients and largely resembles 2D-NMR sequences.

2.3.1 MRI in Medicine

As a non-invasive, non-ionizing imaging method, MRI has become important in many parts of the medical field for example neurology, oncology, cardiology or urology. While the low polarization of nuclei make its sesitivity inferior to other imaging methods such as computed tomography, the nature of the signal generation allow for contrasts that differ vastly from other established mehtods. This uniqueness allows for superior imaging power in many cases despite the smaller sensitvity.

2.3.2 Slice selection

The first step in most imaging methods is to excite a slice of the sample to perform the first spatial selection. To do so, a gradient - mostly in z direction - is aplied to the sample. The following pulses which usually have a limited frequency bandwidth will affect only the nuclei within a slice of the thickness defined by the gradient strength usually given in $\mathrm{mT\,m^{-1}}$ and the pulse's bandwith. It has to be kept in mind that this does not necessarily guarantee that nuclei outside the prepared slice do not contribute to the signal. Movement of parts of the sample such as flow or diffusion can lead to signal artifacts. Furthermore, the following pulses in the sequence have to be carefully designed to not generate FIDs or echos of their own that are not related to the originally selected slice.

2.3.3 Frequency encoding

During readout, a field gradient can be turned on to encode the second spatial dimension. Considering a positive x-gradient, the nuclei at higher x values will then generate a higher frequency than the ones at lower x values and thus show up further right in a 1D-FT.

2.3.4 Phase encoding

Generating an encoding for the third spatial dimension is not quite as straightforward. To do so, a third gradient in a third dimension perpendicular to the two others is necessary. Due to redundancy issues, that gradient cannot simply be turned on during readout though but is used to change the phase of the signal the nuclei generate depending on the position in the sample. That means that the gradient strength needs to be varied to satisfy the sampling conditions for the frequencies generated, i.e. the frequency encoding scheme is run multiple times with a different phase encoding gradient strengths running before it. That way, if the fourier transformed data for each phase encoding step is sorted by gradient strength and fourier transformed in the second dimension, the frequency generated by the more or less quickly changing phase will define the position in y direction.

2.4 Hyperpolarization

The main limitation of NMR and MRI is the low thermal polarization. For each energy state E_i the Boltzmann distribution dictates

$$N_i = \exp \frac{E_i}{k_B T} \tag{18}$$

For energy differences between two states that are small compared to the thermal Energy, the polarization can be expressed as follows:

$$P = N_+ - N_- N = \tanh \left(\frac{\hbar \gamma B}{2kT} \right) \tag{19}$$

2.4.1 Dynamic nuclear polarization

As the gyromagnetic ratio of electrons is much higher than that of any nucleus (factor of 10^3 compared to protons), dynamic nuclear polarization (DNP) uses electrons at low temperatures and high fields to generate large initial polarization. The polarization is then transferred to specific nuclei by microwave irradiation that induces transitions in the spin system of nucleus and electron that is generated by the addition of free radicals. The low temperatures lead to a freezing of the sample and microwaves are applied in that frozen state. For administration, the frozen sample then needs to be quickly melted and transferred, usually in controlled magnetic environments to prevent fast relaxation. The samples can show high polarizations

close to unity but are usually limited by decay during the relatively long delivery times. Efforts building faster transport mechanisms have greatly reduced these times but they stay in the range of tens of seconds.

2.4.2 Hyperpolarization of Noble Gases

2.4.3 Brute Force Hyperpolarization

2.4.4 Parahydrogen induced Hyperpolarization

3 Materials and Methods

3.1 Low field NMR

To achieve NMR spectra at fields where SABRE is feasible **(TODO: Ref sabre)**, a low field NMR spectrometer was built **(TODO: ref niels)**. Its main field is generated by a resisitve solenoid coil. Inside that coil, there is a saddle coil generating a B_1 field perpendicular to B_0. Perpendicular to and inside both, a third coil, also a solenoid, is used to detect the signal generated by the spins.

3.1.1 Static Magnetic Field

Multiple coil designs of the static field generating coils have been considered, simulated, built and tested in the course of this work. The previously used solenoid design with different lengths of compensation windings **??**

Solenoid coil

The B_0 coil is wound around an acrylic tube in two full layers. In addition, at the tube's ends, compensation windings are installed to homogenize the field inside the coil. The length of these windings was optimized in matlab simulations **??** **(TODO: figure of whole setup)** Coils ususally consist of one or more layers of wire usually wound around a PVC tube. Spacing between layers is given by wire thickness including insulation. To keep these distances small and, in turn, magnetic flux density high, enameled wire was used for all coils. Winding of the wire was mostly performed on a turning lathe enabling automatic counting of the number of windings and a steady, cosistent feed of the wire.

Helmholtz Coil

To build a homogeneous dual helmholtz array, simulations were also considered. as space was limited inside the Mu metal shield the coil was also supposed to be used

in, the coils' diameters were predetermined and only the coils distances and currents were optimized (see 4.1.1 for details). As the general setup, a PVC tube onto which are slid four coil holders was chosen. Using the simulation results, a layout for the coil holders was designed. To keep unwanted fields due to connecting wires to a minimum, these wires were kept as short as possible. Holders were lathed and then processed furhter by hand. Winding of the wire was also done by hand. To keep the wire form sliding into the gouges of the previous layer, PVC foil was lasercut to fit the dimensions of the coil holders. Due to the limited size of the foil used (Din A4) and the relatively large diameter of the coils, three stripes of foil were connected with one of the three parts employing a feedthrough for the wire transversing from one layer to the next.

3.1.2 Radiofrequency Excitation

To irradiate samples with radiofrequency pulses, a saddle coil **(TODO: dimensions)** wsa used. It was operated untuned and unmatched as a broadband resonator. The pulse generation was performed using a National Instruments data acquisition crate (NI **(TODO: which?)**).

3.1.3 Software control

All software control was realized using Matlab in combination with the DAQmx libraries. The prevoiusly existing code was strongly modified in the course of this work to implement more features and fix buggy behaviour.

3.1.4 Data Readout

All readout was done using a 12 bit NI **(TODO: name)** card operating 10 MS/s. The signal was recorded directly without preamplification or mixing. That required small distances between readout coil and NI card to keep signal losses at bay.

3.1.5 Shim System

For homogenization of the field, a shim system was built according to Biot Savart simulations. It features linear shim coils for all three spatial dimensions mounted to a .**(TODO: cm)** acrylic tube. The x and y shims are made of four saddle coils respectively that were plainly manufactured individually and bent to fit the tube. The

z shims, which are basically a pair of maxwell coils, were added on top of these saddle coils. All shims are driven by a **(TODO: H&U)** programmable power supply providing up to $10\,\text{A}$ of current. The power supply is connected via a virtual serial port inside a USB connection. That way, the three shim channels can be controlled from inside the Matlab hypercontrol program **??**

3.2 Magritek Low Field MRI

To acquire images at low fields, a Magritek Terranova **(TODO: ref)** was used. It features similar hardware as the low field spectrometer, but uses its B_0 coil only for prepolarization while signal is acquired at Earth magnetic field. **(TODO: subsections)**

3.3 Bruker Low Field MRI

3.3.1 Gradient Coil Setup

3.3.2 Signal mixer

3.3.3 Receive coil

3.3.4 Paravision and Topspin software

3.4 High field MRI

The most well known application of NMR is the high field MRI of human antomy with its widespread use in clinics around the world. Not as common, but equally important are preclinical scanners for research purposes. These preclinical scanner, primarily built for animal experiments, were used in most of the high field experiments shown in this work.

3.4.1 MRI Hardware

For the acquisition of spectra and images, hardware for different purposes is requred:

- B_0 field generation

- Pulse generation

- Field gradients generation

- Signal readout

3.4.2 Paravision Software

The stadard Bruker imaging software called paravision features sequence and method implementations for the more common use cases and can additionally be modified for specific purposes. Sequence programming is generally in C++ while many other modifications can be done via GUIs. For the purposes of this work, the most common sequences were rather simplistic NMR sequences while some images of hyperpolarized tracers have been generated with more sophisticated imaging sequences.

3.4.3 Custom High Field Coils

Most commercially available coils are for proton imaging and spectroscopy. Coils for other nuclei are obtainable, but usually expensive and not necessarily tailored to the specific purpose in mind. Therefore, we built single and dual tune coils for different nuclei and different fields.

^{15}N **coil**

A solenoid of thick, stable copper wire was wound to fit the experimental setup of the shuttling system described in 3.5. The solenoid was attached to a circuit board via clamped and soldered connections. On the board, a high voltage tune capacitor as well as two symmetric matching capacitors were installed. Coaxial cable was used to make the connection to the scanner and the whole setup was mounted to a teflon holder for precise positioning. The tune capacitor was chosen so that it can be tuned to both a $7\,T$ and a $9.4\,T$ field at $300\,MHz$ and $400\,MHz$ respectively. **(TODO: image coil)**

3.5 Shuttling system

To measure in-situ Sabre polarized substances at high fields, a transfer system is necessary. This system can either move a probe inside a closed container **??** or transfer the probe itself via tubings. We chose the latter for the more flexible and

less difficult positioning especially in the environment of a lieing bore small animal scanner as compared to a standing bore spectrometer. In addition, all actuation can be done by non-magnetic gases which was beneficial especially at the $9.4\,\mathrm{T}$ machine which is unshielded and creates $5\,\mathrm{G}$ fields in a distance of about $1\,\mathrm{m}$ from the scanner bore.

3.5.1 Magnetic Shielding

To be able to polarize ^{15}N using Sabre Sheath **??**, fields of the order of magnitude of $100\,\mathrm{nT}$ were necessary. Thus, Earth magnetic field needed to be shielded against. To do so, we purchased a three-layered Mu-Metal shield (ZG-218, Magnetic Shield Corp.) with shielding factors of 100 per layer.

3.5.2 Low Field Reactor

At low field, multiple design features have to be combined to achieve high polarization yields. First off, pH2 has to be supplied to the sample continuously and efficiently. Positioning of the probe has to be reproducible to ensure the fields are well defined. The system must be resistant to the chemicals and solvents used in the experiments and hold the pressures applied during measurements. Furthermore, it must be non magnetic to not distort residual fields inside the shield which otherwise might reduce polarization in parts of the sample. To fulfill all these requirements, polysulphone (PSU) was chosen as a material because of its high mechanical and chemical stability. The reactor was designed in Inventor (Autodesk) as a body of rotation. It features a sample volume of about $3\,\mathrm{mm}^3$ with a larger diameter venting area to reduce sample losses due to foaming and spray. Below the sample volume, a interchangable punched disk is installed that provides pH2 to the sample in fine bubbles. By changing the number and diameter of the holes, flow rate and bubble sizes can be adapted to provide pH2 effectively to different kinds of samples and under different conditions.In case of sample transfer, the conical bottom collects the sample for an efficient and complete sample extraction. Two lines connect to the bottom: one to supply pH2 gas and the other to transfer the sample towards the high field. An additional gas line connects to the top of the venting area for both de- and pressurization of the sample chamber.
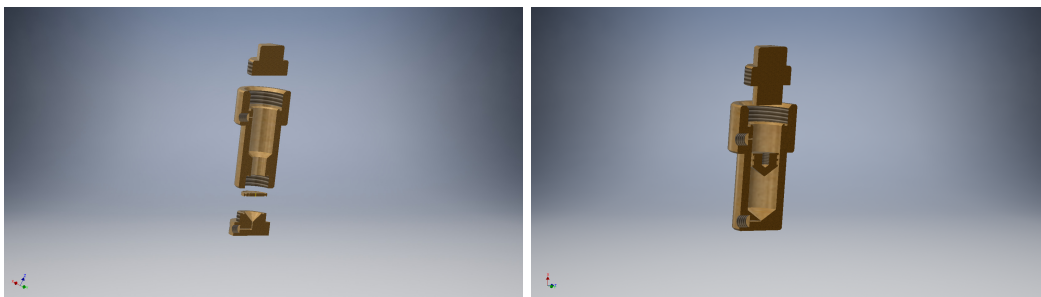
Figure 1: Half cut views of the low field reactor (left) and high field probe (right). The disk for pH2 provision in the low field reactor is visisble on the bottom sandwiched between the main body and the screw on cap. Hose connections are made to that cap and the top of the main body. The high field probe is shown with its optional piston inserted, the two possible connections at the top for actuation and bottom for sample transfer are visible.

3.5.3 High Field Probe

Similarly to the one in low field, the high field probe has to withstand the high pressures applied and the chemicals used. It is made from the same material, PSU. While its conical bottom is similar to the low field probe's, there's no need for a bubbling system. There are two procedures for shuttling the solution back to low field: Via a piston that can also be actuated by pressurized gas or simply by the gas pressure that builds above the solution due to the transfer towards high field. With methanol solutions, the latter method turns out to be efficient, other solutions with different viscosities may need the piston approach for efficient transport.

3.5.4 Fluid handling system

Sample volumes range in the ml regime thus sample losses are unfavorable.

3.6 Fluxgate Field Probe

3.6.1 Arduino Shield

3.6.2 Teensy 3.6

4 Simulations

4.1 Biot Savart field simulations

4.1.1 B_0 fields in low field NMR

For B_0 field generation, mostly solenoid coils with compensation windings on both ends were used. To find optimal lengths and numbers of layers, Matlab simulations of static fields using Biot Savart's law were implemented. Both solenoidal structures and "closed" loops were simulated. The measure considered was absolute field distribution inside a volume of $3\,\mathrm{cm}$ by $3\,\mathrm{cm}$ by $3\,\mathrm{cm}$. fields were calculated in a grid of **(TODO: 30 cubed)** points. Absolute field difference inside the volume was considered first and then refined by histogram evaluation which yields results similar to the lorentian distribution a fourier transformed NMR signal shows. To estimate linewidths generated by field inhomogenyeties, the conservative measure of the central 80 % of field points was used. Using this representation and varying different parameters such as diameter, distances and relative currents in different loop structures, optimal geometries for different coil designs were calculated.

4.1.2 Solenoid Coil

The field of an infinitely long solenoid would be almost perfectly homogeneous along its symmetry axis. Due to the limited

4.1.3 Additional Compensation Windings

Additional compensation windings further smoothed the field by adding a differently shaped field component that can be used to partly compensate the solenoids inhomogenieties. Figure **(TODO: nn)** shows the fields of solenoid and and compensation windings in the x-z-plane and the resulting superposition. To evaluate the field in the 3D sample volume, histograms of the field distribution were generated for different compensation wind lenghts. As visible in figure nn, the influence of a single wind are

quite substantial indicating that the manufacturing process must be well controlled. Additionally, it can be seen that

4.1.4 Dual Helmholtz Array

As a more advanced setup that is less prone to manufacturing errors due to the relatively larger distances to the sample volume, a dual helmholtz array design was considered. A single Helmholtz array provides less Homogeniety than a solenoid (Fig ..) but the additional pair of coils generates a differently shaped field similar to the compensation windings for the solenoid. By variation of the distances of both pairs relative to the center and their respective field strengths, i.e. the currents of the coil pairs, optimal parameters were extracted from the simulations. The

4.2 Simulations using the groups' spin dynamics(TODO: name?) framework

To estimate the

5 Results

As a large part of this work consisted of hardware design and manufacturing, I will split the results section into sole hardware results and measurements with said hardware.

5.1 Hardware

5.1.1 Low field NMR

Receive coils

Receive circuits provided q-factors of **(TODO: measure)** resulting in resonances about $1\,\mathrm{kHz}$ wide. Note that the connection to the NI DAQ introduces additional capacities and inductances that cannot be neglected especially in the higher frequency range above $100\,\mathrm{kHz}$ where the coil's intrinsic capacities are comparatively small.

$\mathrm{B_0}$ coils

The manufactured $\mathrm{B_0}$ coils show fields (i.e. frequencies) as well as linewidths in the order of magnitude the simulations predicted. Through manufacturing errors, and changes to the coil in long term use cases, the linewidths deteriorated. It is important to note that, at currents above $1\,\mathrm{A}$, the $\mathrm{B_0}$ coil heated noiticabely. while the heating itself is unproblematic, the resulting exansion of the materials leads to an overall longer coil and thus lower fields **??**fieldSolenoid). To avoid field shifts during measurements, the setup should therefore be in thermal equilibrium. This is especially relevant when switching fields during measurements using the programmable power supply.

5.1.2 Shims and programmable power supply

The three linear shims are settable via the programmable power supply and show their expected effect. The rotational position of the receive coil is relevant to the

shims indicating they're working as intended. Using the added shim tool, line widths were reduced from $\approx 250\,\mathrm{Hz}$ to $\approx 30\,\mathrm{Hz}$ in the case of large samples of $\approx 40\,\mathrm{ml}$. If the initial field was generated by a less homogeneous, more asymmetric coil in which no signal was visible without shims, signal was discovered and linewidths went down to $\approx 50\,\mathrm{Hz}$.

5.1.3 Sabre shuttling system

The system designed to transfer a sample between fields works as intended. Fluid losses are small and acceptable with about **(TODO: how much)** lost within **(TODO: nn)** shuttling cycles. The bubbling system works well and provides pH2 to the solution in large amounts. The pressure stability of the vessels has been tested to withstands up to $50\,\mathrm{bar}$. Chemical resistance is good though resistance to pure pyridine is not given. While there was never any problem with the mM pyridine concentrations used in the experiments, a neat pyridine batch showed to dissolve the PSU casing.

5.1.4 Fluxgate readout electronics

The readout electronics were designed to feature a wide range of amplifications for all three spatial dimensions. A 24 V DC power supply was fitted with a DC-DC-converter to provide the $\pm 15\,\mathrm{V}$ to power the Fluxgate. Additionally the PCB board was fitted with the electronic parts (see 3.6). For testing purposes, a simple program using serial in and output to toggle the analog switches was written. All switches were successfully tested to work, though three had to be replaced at some point for malfunction. Apparently this was due to damage during assembly as the board is now working as expected.

5.1.5 Fluxgate calibration

The three spatial channels of the fluxgate sensor needed to be calibrated as to their intrinsic offsets as described in **??**. Data for X- and Y-channels are shown in figure **??** The fit parameters shown in table **??** allow for calibration of X- and Y- channel by calculating the average offset for all Positions. Using the data for calibration, the measurements of the X- and Y-channels can be used to plot a 2D-section of the field using the phase of the fit as the field direction and the amplitude as its magnitude. Both X- and Y-sensor are shown in figure **??**. The absolute positions

position	1	2	3	4	5	6
amplitude	22.4	27.0	35.9	39.6	45.2	42.5
offset						
phase						
position	7	8	9	10	11	
amplitude	42.9	45.1	45.4	44.6	40.6	
offset						
phase						

are indicated in the figure to enable comparison of the individual results in the same absolute position. The same data is also shown in a 3D plot (fig. **??** to show the field progression inside the mu metal shield.

5.2 Measurements

5.2.1 Low field NMR

Low field spectra were acquired using different setups. The main modification between setups concerned the B_0 coil. The initially used solenoid coil showed linewidths of about 0.5 - 1 kHz. Due to mechanical destruction of one coil and those rather wide lines, a new coil design was simulated and built 4.1.4 using Biot Savart calculations.

5.2.2 Sabre in water

5.2.3 Sabre in cell solution and blood

5.2.4 15N Sabre

15N coil

The coil for 15N signal reception was matched and tuned to fit the requirenst of the system. The network analyzer showed a q-factor of **(TODO: n)** and a width of nn. Inside the small animal NMR, similar resonance widths of nn were observed while the attenuation was $1\,\mathrm{dB}$

Shuttling reproducibility

To ensure that the sample is removed completely from the high field side, spectra in both 'states' of the system were recorded (**??**. Integration over both spectra yielded

a upper limit of sample remaining inside the high field chamber of which corresponds to an effective polarization reduction of 1%. To test the reproducibility of the shuttling system, a hyperpolarized 1H pyridine sample was shuttled back and forth multiple times. The results of the measurement are shown in figure **??**.

5.2.5 Nanotesla field measurements

The field inside the Mu Metal shielding was measured without anny current flowing in the B0 coil as well as with the coil turned on.

5.2.6 High field Sabre

5.3 Simulations

5.3.1 Static magnetic field calculations

Using the Biot Savart law, a Matlab program to calculate the fields of current carrying conductors was implemented. Structural elements were mostly solenoids, but also saddle and helmholtz coils were considered.

solenoid coil

The coil used in the low field NMR system was calculated and the length of the compensation windings was optimized for field homogeniety. To do so, the field was calculated inside a $3x3x3cm^3$ volume centered inside the coil and plotted as histograms binning fields. An algorithm analyzing over which field 80% of the fields sampled spread was used as a marker

Helmholtz Array

The previously used program was also used to simulate the field of the helmholtz array used in later experients. The simulations were used to optimize the parameters for the setup before manufacture. The simulation results concerning the positions of the coils are shown in figure **??**. The optimal result is marked, and the field homogeniety is plotted for this result (figure **??**). Comparing the field map to figure **??** shows a factor **(TODO: nn)** improvement.
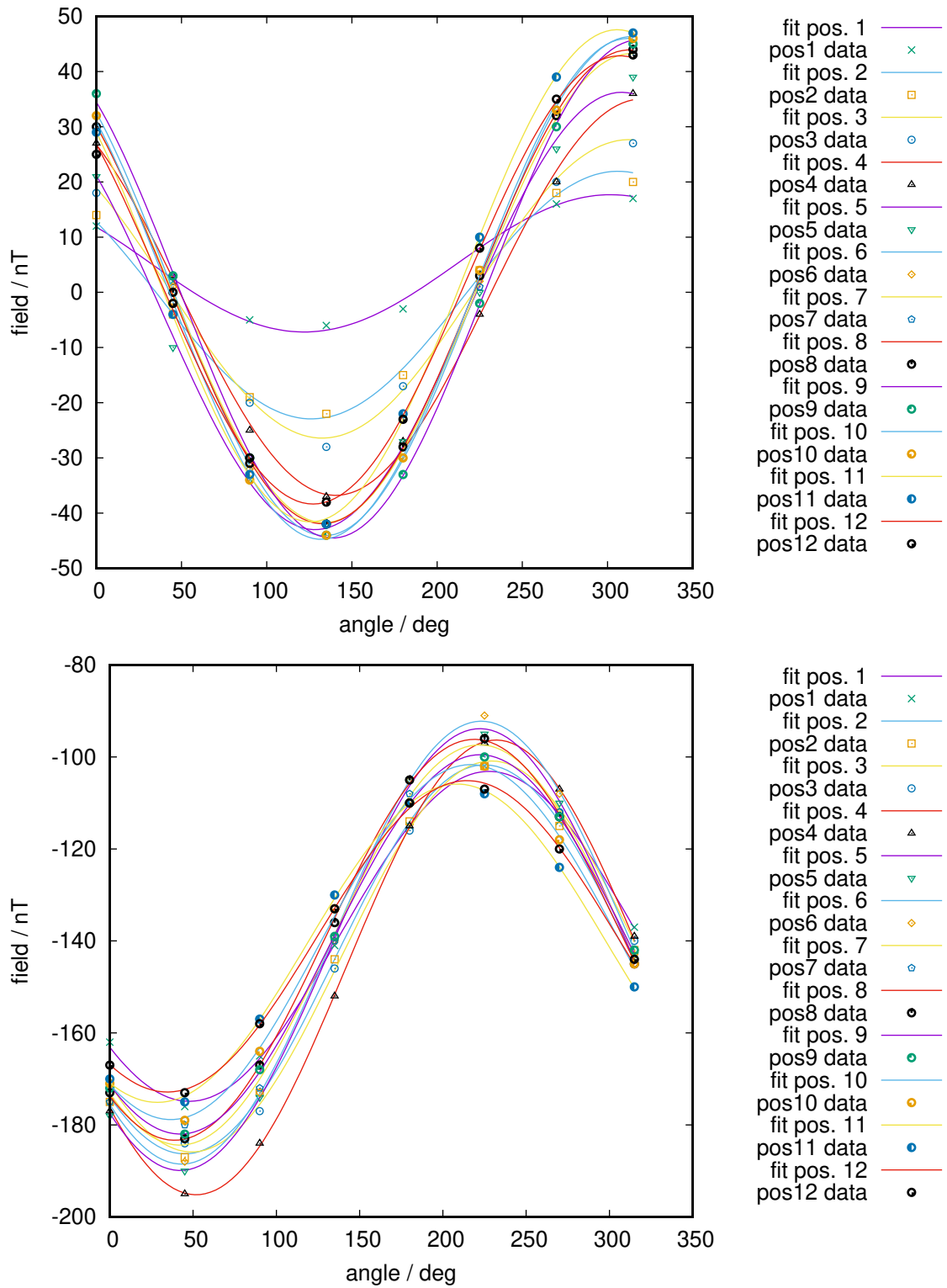
Figure 2: Calibration data of X- and Y-channel. Each dataset in the key corresponds to a full rotation at one position in the MuMetal shield. The solid lines correspond to a sine fit to each dataset with phase, amplitude and offset as fitting parameters. Error bars are not displayed for better visibility. 25
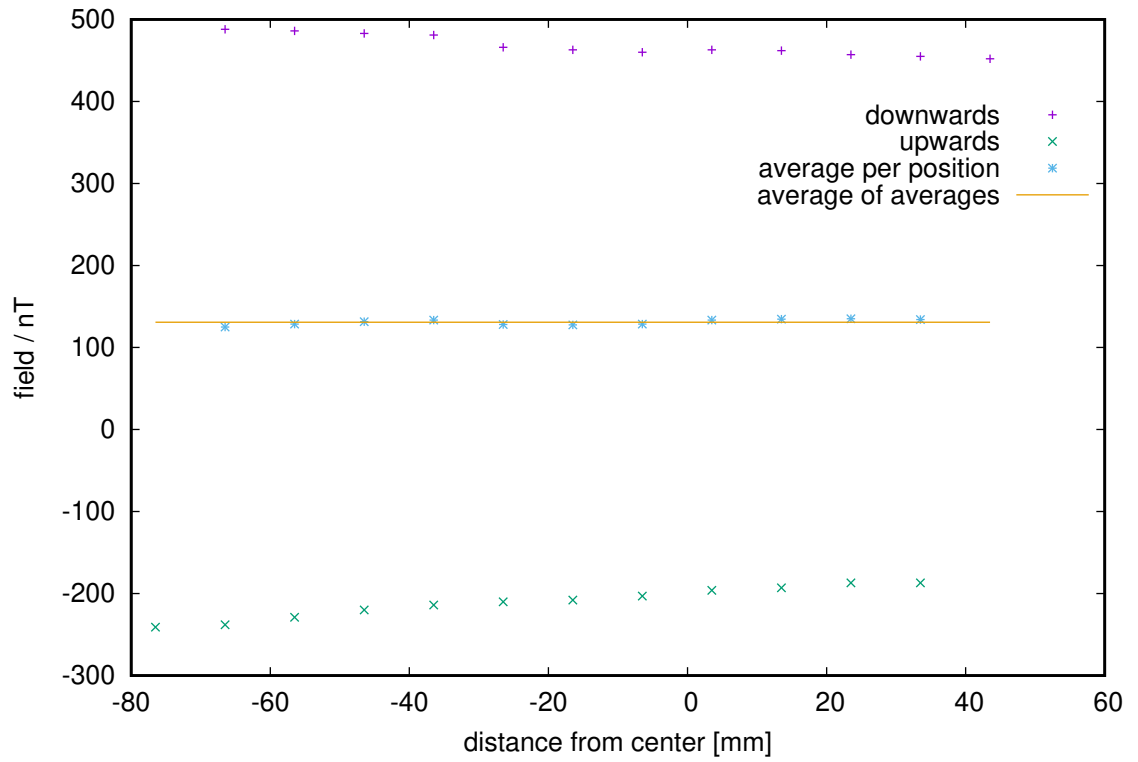
Figure 3: Calibration of the Z-channel. Due to spatial limitations, no full rotation in z direction was possible. The two datasets represent one measurement in "upwards" ond one in "downwards" direction. The solid line represents the average of the positional averages of the two directions.
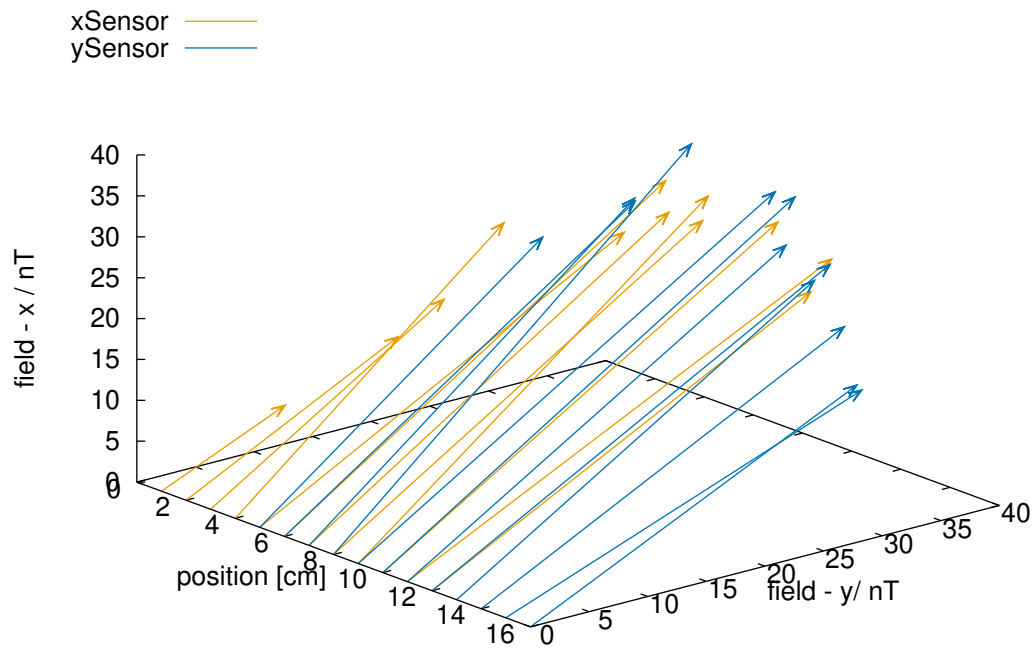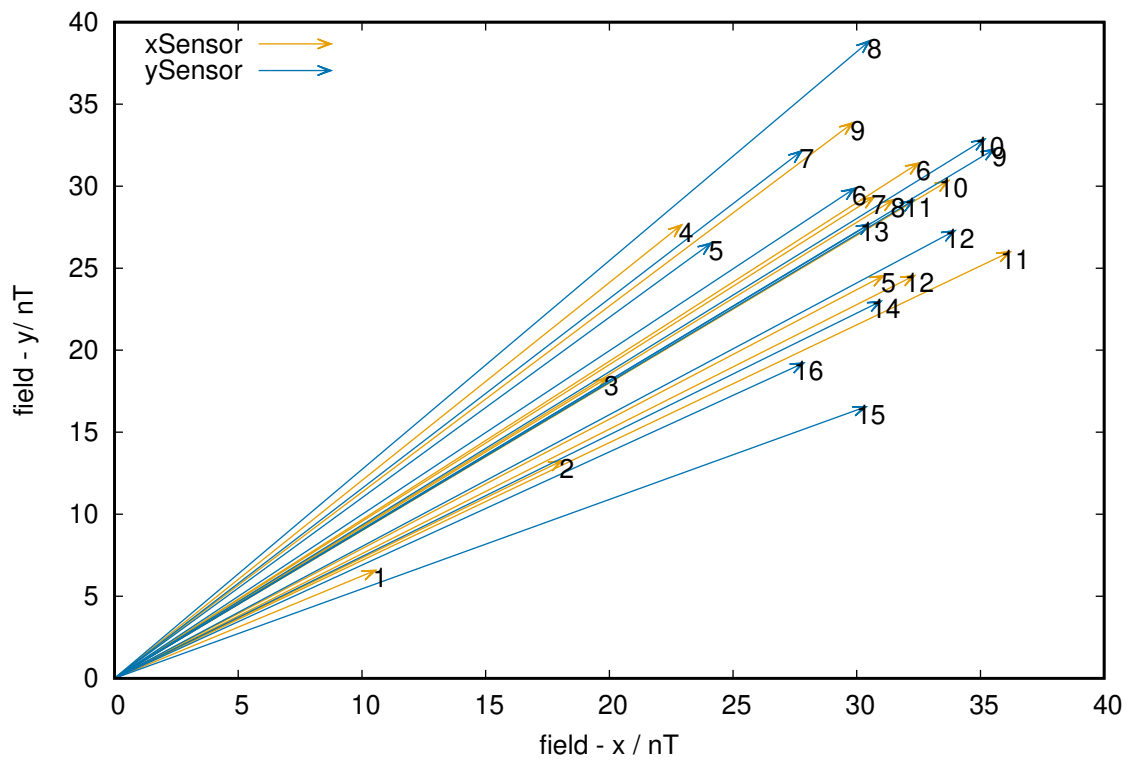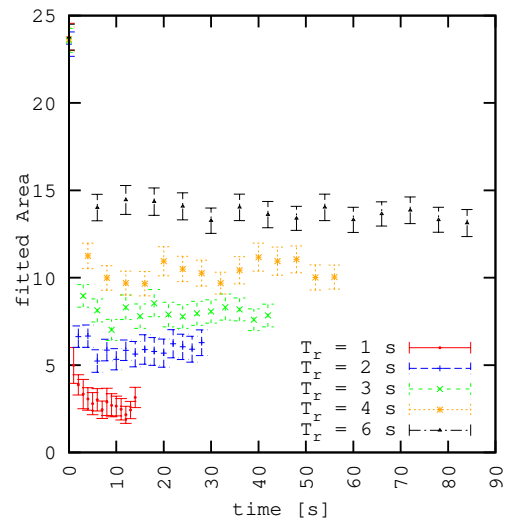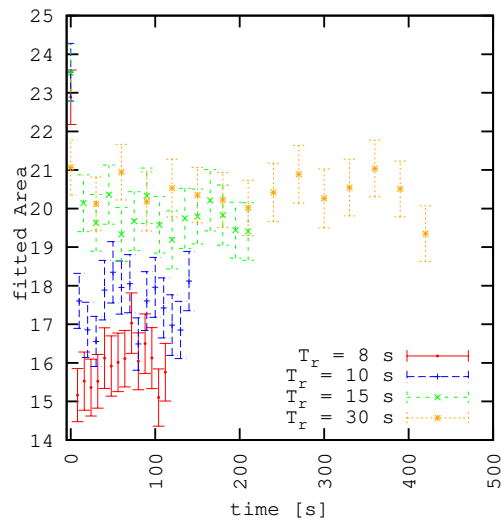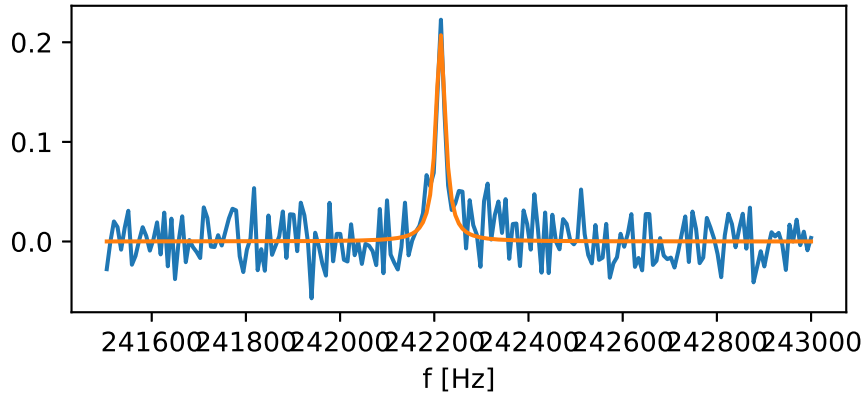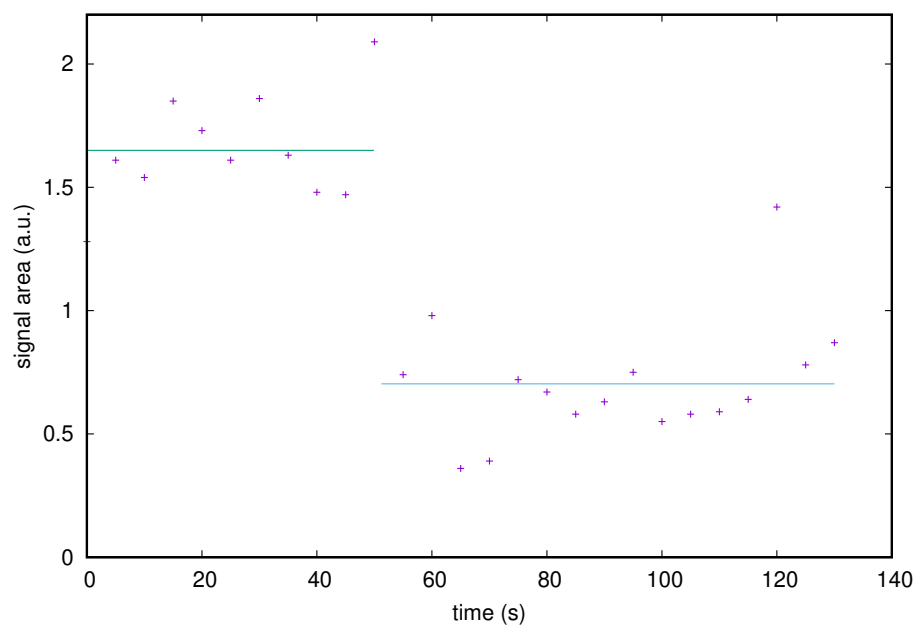
Figure 4: Time course of the signal intensity (peak height) when adding human blood to the continuously hyperpolarized solution. Note the string signal drop after addition of $0.5\,\mathrm{ml}$ of blood to the solution. The straight and dashed lines indicate the average before and after blood addition.
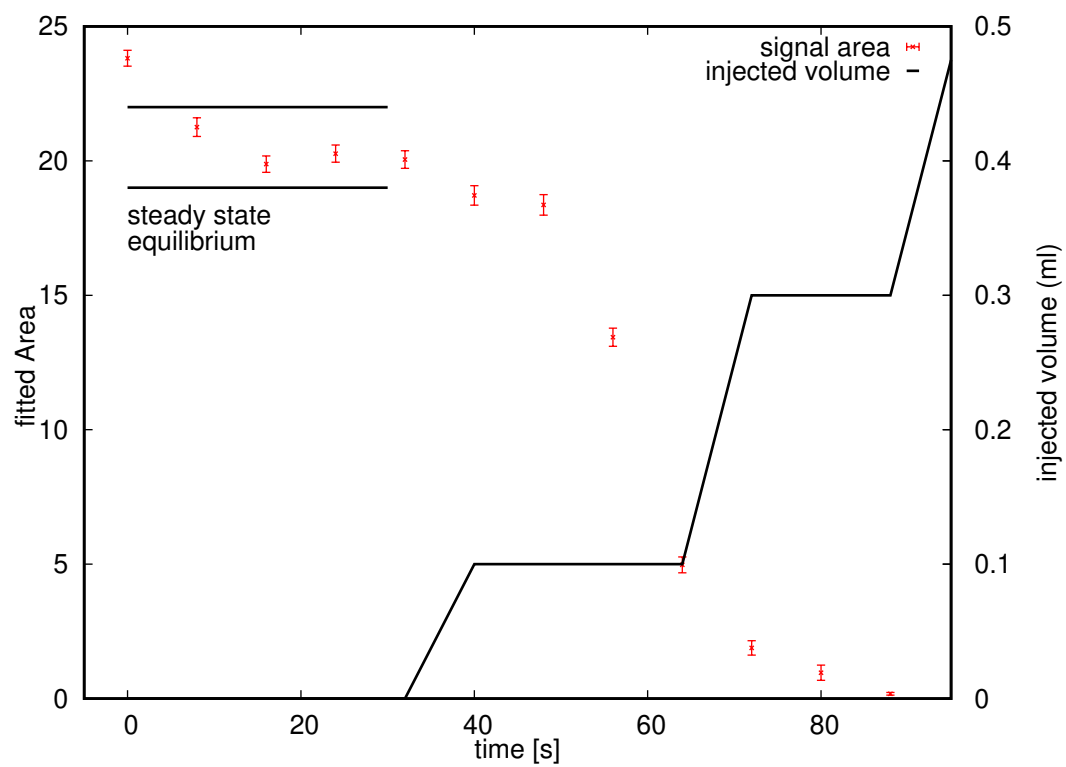
Figure 5: Signal drop during the injection of $0.5\,\mathrm{mL}$ of blood into the solution providing hyperpolarized signal which was permanently provided with fresh pH2.
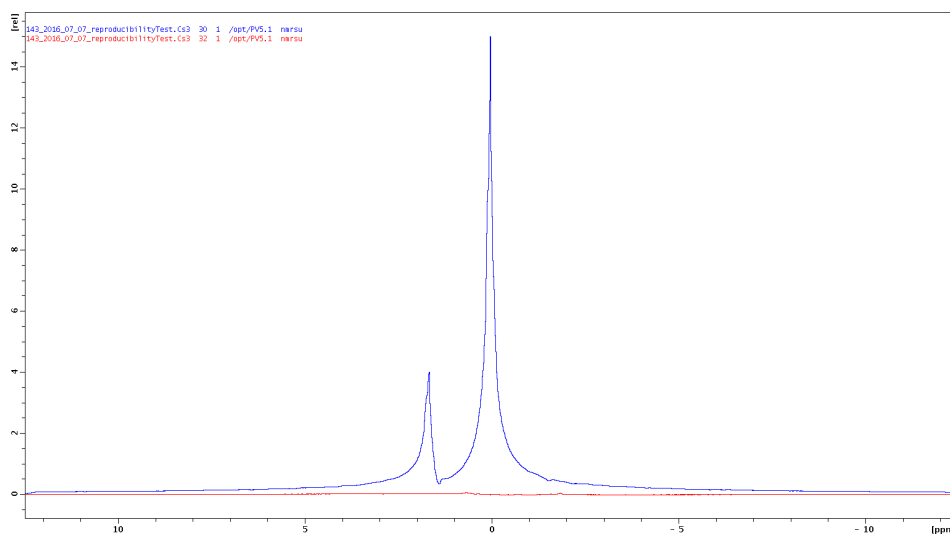
Figure 6: 1H spectra of the high field reactor in the filled (blue) and empty (red) state. The filled state delivers a lot more signal as expected while the integration over the empty state spectrum shows a signal reduction of 1000.
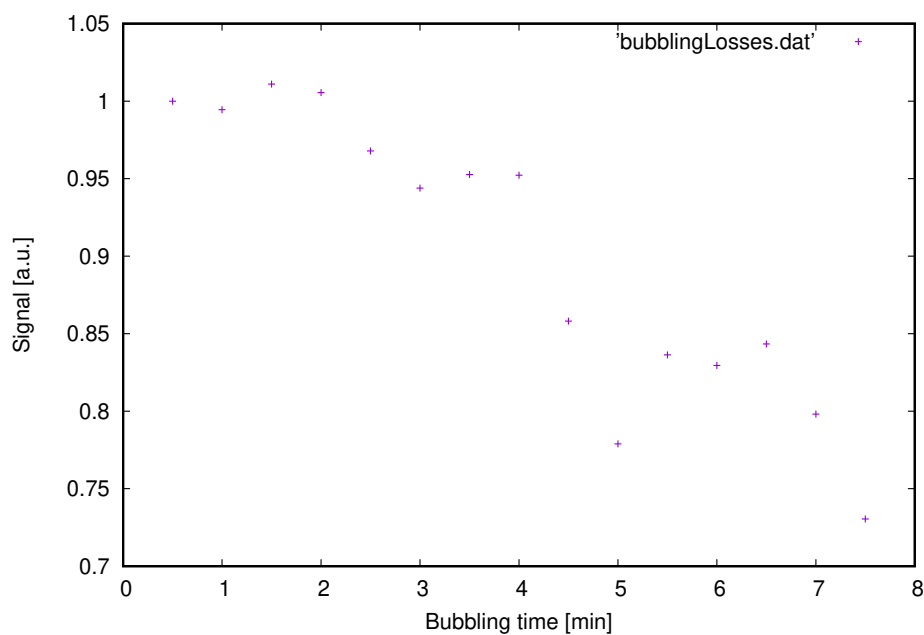
Figure 7: Signal intensity during multiple minutes of hydrogen bubbling using a hyperpolarized 1H-pyridine sample. Note that the signal drops to about 70 % of its initial value after 8 minutes of continuous hydrogen supply. The initial rise of signal during the first two minutes indicates a temperature effect unaccounted for.
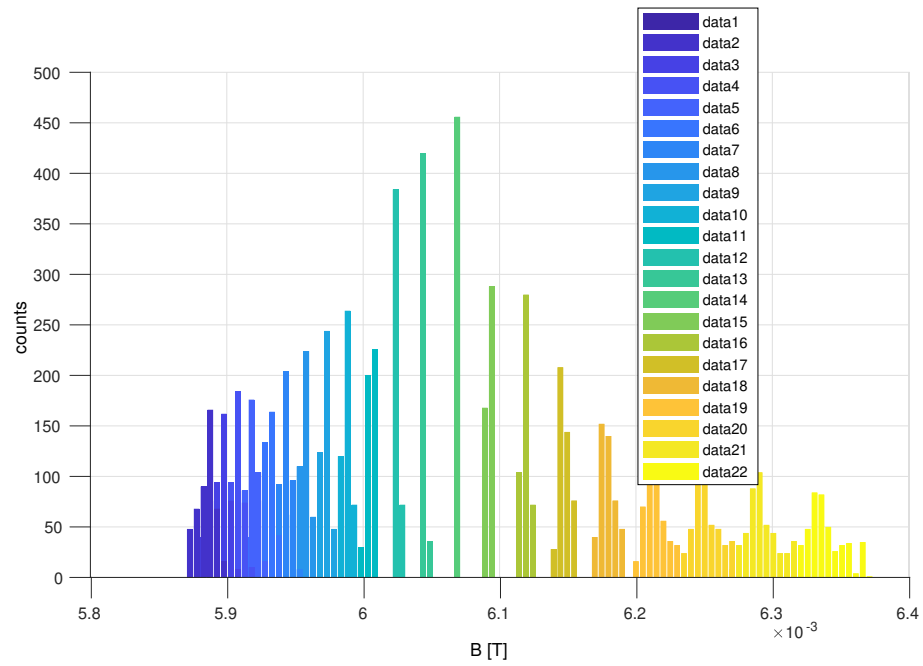
Figure 8: Histograms of the magnetic field strength. From left to right, number of compensation windings rise. This leads to a field increase and change in homogeniety.
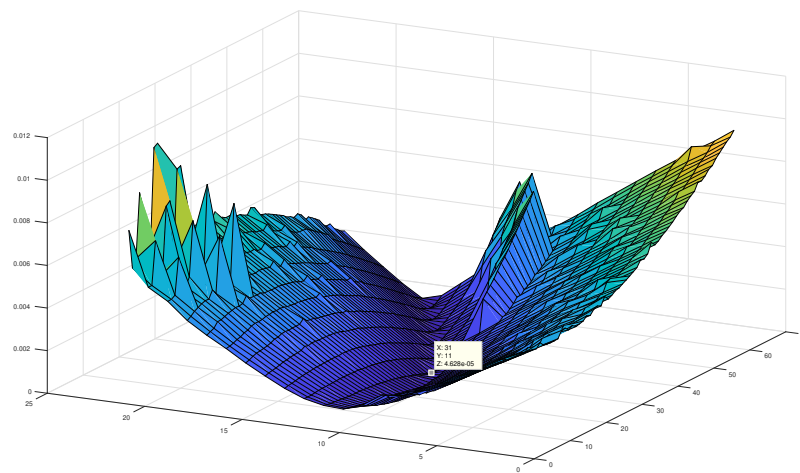
6 Conclusion

6.1 B_0 field generation

Multiple coil designs of the static field generating coils have been considered, simulated, built and tested in the course of this work. The previously used solenoid design with different lengths of compensation windings **??** showed rather broad lines in both simulations and measurements. Main reason are the discrete number of compensation windings that do not allow for fine enough tuning of the coil. This could be improved by putting the compensation windings on sliders that can move in z-Direction. additionally in the design used, mechanical errors in the build worsened the problematic. Due to the high number of windings guided only by the previously wound wire, shifts building along the coil's z axis are inevitable. In addition, layering the wire leads to slippage into the gouge created by the previous layer. This problem may be solved by using a thin, but stiff layer of material to separate the wire layers from each other. All of the mentioed solutions are inconvenient when considering the dimensions of the coil.

The dual helmholtz arary design deals with the above mentioned problems. The single coils are wound onto a milled holder making moving in z direction possible and convenient. due to the shorter extension of the coils in z direction, the errors introduced in the winding process are smaller and using PVC foil to separate the axial layers kept the layers neatly wound. In addition, the design allows for axial access to the sample which can make experiments a lot more convenient. The disadvantage of the design are the higher currents due to the lower winding count that make need for higher current power supplies.

6.2 B_1 coils

7 Acknowledgments

First and foremost, I would like to thank...

- advisers

- examiner

- person1 for the dataset

- person2 for the great suggestion

- proofreaders

Bibliography

[1] J. Bromley, J. W. Bentz, L. Bottou, I. Guyon, Y. LeCun, C. Moore, E. Säckinger, and R. Shah, "Signature verification using a "siamese" time delay neural network," *International Journal of Pattern Recognition and Artificial Intelligence*, vol. 7, no. 04, pp. 669–688, 1993.

[2] D. Kingma and J. Ba, "Adam: A method for stochastic optimization," *arXiv preprint arXiv:1412.6980*, 2015.